

Band bending engineering in p-i-n gate all around Carbon nanotube field effect transistors by multi-segment gate

Ali Naderi^{1*}; Behrooz Abdi Tahne²

¹Electrical and Computer Engineering Faculty, Kermanshah University of Technology, Kermanshah, Iran

²Young Researchers and Elite Club, Kermanshah Branch, Islamic Azad University, Kermanshah, Iran

Received 16 April 2017;

revised 06 July 2017;

accepted 18 August 2017;

available online 29 August 2017

Abstract

The p-i-n carbon nanotube (CNT) devices suffer from low ON/OFF current ratio and small saturation current. In this paper by band bending engineering, we improved the device performance of p-i-n CNT field effect transistors (CNTFET). A triple gate all around structure is proposed to manage the carrier transport along the channel. We called this structure multi-segment gate (MSG) CNTFET. Band to band tunneling (B-B tunneling) is a dominant transport mechanism in p-i-n structures which is more controlled here by band bending engineering. Gate metal at source side causes more bands bending at channel to source interface and the gate metal at drain side acts as a filter which reduces the leakage current. Results demonstrate that by parameter engineering of gate metal, the proposed structure improves the saturation current, leakage current, current ratio, subthreshold swing, breakdown voltage and cut-off frequency in comparison with conventional structure. Also, to obtain the optimum parameters, design considerations has been done in terms of difference in workfunctions and change in the length of each part of gates. Simulations and comparisons have been performed using none equilibrium Green's function and self-consistent solution between Poisson and Schrodinger equations.

Keywords: Current Ratio; Cut-off Frequency; Leakage Current; MSG-T-CNTFET; NEGF; Saturation Current; Subthreshold Swing.

How to cite this article

Naderi A and Abdi Tahne B. Band bending engineering in p-i-n gate all around Carbon nanotube field effect transistors by multi-segment gate. *Int. J. Nano Dimens.*, 2017; 8 (4): 341-350.

INTRODUCTION

Tunneling field effect transistors are attractive devices for low power electronic applications. Their low subthreshold swing and high subthreshold slope make them a good candidate for short channel devices. Beside these desirable characteristics, they suffer from some drawbacks such as ambipolar behavior and low saturation current (I_{ON}). High current at ambipolar regime results in some challenges for circuit design such as creation of large parasitic current and failing in determined performance of circuit [1]. CNTs, in addition to their wide applications in other aspects of technology and industry, are promising building block for future nanoelectronics [2-6]. Due to the small diameter (1 nm), CNTs are ideal candidates to study one-dimensional (1-D) electrical transport phenomena, even at room temperature. CNT

transistors have generated considerable interest in the past few years because of their quasi ideal electronic properties [3, 7-9].

Recent advances in carbon nanotube field effect transistor (CNTFET) engineering results in attractive DC characteristics for this type of transistors [10]. Tunneling CNTFETs (T-CNTFETs) or p-i-n (or n-i-p) devices are using combined benefits of both CNTFETs and tunneling devices, simultaneously. To improve power consumption and saving energy the T-CNTFETs were proposed and investigated. T-CNTFETs enjoy much better subthreshold swing than the MOS-like structure [11-13]. As stated before, beside desirable characteristics, T-CNTFETs suffer from drawbacks such as ambipolar behavior and small saturation current leads to low current ratio [14]. Researchers have investigated and proposed some novel structures to improve the

* Corresponding Author Email: a.naderi@kut.ac.ir

Here, the diagonal factor U_j matches to the on-site electrostatic potential along the tube surface calculated by solving the Poisson equation. In equation (4), q is quantum number, $t=3\text{ eV}$ is the nearest neighbor hopping parameter, $b_{2q}=2t\cos(\pi q/n)$, N is the whole amount of carbon rings along the transistor, and n is CNT index equal to 13 here. We are solving the problem in mode space where we have A and B-type rings [20]. The odd-numbered diagonal entries refer to the A-type submatrix and even numbered ones to the B-type submatrices. In mode space, where q is an integer (quantum number), each A-type point couples to the next B-type point with the parameter, b_{2q} and to the previous B-type with the parameter, t . Similarly, each B-type ring couple to the next A-type ring with parameter, t and to the previous A-type ring with parameter, b_{2q} [20].

The retarded Green's function is computed by [14]:

$$G_q(E) = [(E + i\eta^+)I - H - \sum_s - \sum_D]^{-1} \quad (5)$$

we have considered self energies (Σ_S, Σ_D) for semi-infinite leads as boundary conditions. In this equation I is unity matrix and η^+ is infinitesimal number.

In these circumstances we can consider that CNT is connected to considerably lengthy CNTs at its end. All in entries of source self energy function (Σ_S) are zero excluding the (1, 1) component [14, 15]:

$$\sum_{s(1,1)} = \frac{(E-U_1)^2 + t^2 + b_{2q}^2 \pm \sqrt{[(E-U_1)^2 + t^2 + b_{2q}^2]^2 - 4(E-U_1)^2 t^2}}{2(E-U_1)} \quad (6)$$

In the same way, Σ_D has just its (N, N) component nonzero, and it is given by an equation like equation (5) with U_1 substituted by U_N .

By using the calculated charge and solving the Poisson equation the fresh electrostatic potential is developed. The iteration between Poisson and Schrodinger equations continues until the self-consistency is attained. After self consistency, the current is calculated by [7, 14, 15]:

$$I = \frac{2q}{h} \int T(E) [F(E - E_{FS}) - F(E - E_{FD})] dE \quad (7)$$

This equation is known as Landaur-Buttiker formula. The $T(E)$, which is transmission coefficient, is calculated from the following equation:

$$T(E) = \text{trace}(\Gamma_S G \Gamma_D G^+) \quad (8)$$

$E_{FS} (E_{FD})$ is source (drain) Fermi level, h is Planck constant, G is Green's function, $\Gamma_{S(D)}$ is the energy level broadening due to source (drain) contact and

is calculated as:

$$\Gamma_{S(D)} = i(\sum_{S(D)} - \sum_{S(D)}^+) \quad (8)$$

The band structure of CNT can be found from the band structure of graphene. The two-dimensional dispersion (E-K) relation of graphene can be obtained using tight-binding approximation [20]:

$$E_{\text{Graphene}}(k_x, k_y) = \pm t \left[1 + 4 \cos\left(\frac{3k_x a_{cc}}{2}\right) \cos\left(\frac{\sqrt{3}k_y a_{cc}}{2}\right) + 4 \cos^2\left(\frac{\sqrt{3}k_y a_{cc}}{2}\right) \right]^{1/2} \quad (9)$$

Where a_{cc} is inter-atomic distance, the k is wavevector and t is the transfer integral (or nearest-neighbor parameter), the positive and negative terms correspond to the symmetrical bonding and antibonding energy bands respectively. The band structure of the SWCNT is calculated by imposing periodic boundary conditions around the circumference of the tube, i.e., the wave function has to be single valued

$$e^{ik \cdot r} = e^{ik \cdot (r + C_n)} \quad (10)$$

Where C is chiral vector, k is a wavevector and r is a real space lattice vector of the graphene lattice (only the plane wave part of the Bloch wave function written here). This leads to periodic boundary condition in momentum space [20].

$$k \cdot C_n = 2\pi p \quad (11)$$

Where p is an integer. Band structure can be plotted from above equations. The absolute value of electric field is the derivative of energy band diagram. So, electric field distribution can be found along the device.

RESULTS AND DISCUSSIONS

Output currents versus drain source voltage at different gate source voltages are illustrated in Fig. 2. These characteristics have obtained for 15 nm gate length and 0.3 eV difference between the workfunction of side gates and the middle one. As we mentioned before, the side parts of gate have equal workfunctions. It is obviously seen that the proposed structure has higher saturation current. This is a valuable improvement for MSG structure where the lowest saturation current of this structure is higher than the maximum value of current for conventional structure in the range of 0.4 to 0.6 V for gate source voltage. For example to get about 1 μA saturation current, the proposed structure just needs 0.4 V bias, while the conventional structure needs more than 0.6 V

bias. Fig. 3 demonstrates that the MSG structure lowers the threshold voltage and increases the potential barrier sensitivity to gate voltage. This specification is useful for many requests such as sensor applications where a small change in voltage can be properly sensed by larger variation in output current which shows more sensitivity to diagnose the change in signals [6].

Fig. 4 illustrates the energy band diagram for both structures at $V_{GS}=V_{DS}=0.4$ V. MSG structure increases the band bending at source side of channel and amplifies band to band tunneling (B-B tunneling) at ON regime. This is the reason for larger saturation current of MSG-CNTFET.

Fig. 5 shows the $I_{DS}-V_{GS}$ characteristics of the

structures at different drain source voltages. This figure is the logarithmic scale presentation of Fig. 3. It is seen that the proposed structure lowers the leakage current.

To investigate the reason for this improvement, Fig. 6 shows the band diagrams at OFF regime. The large amount of leakage current in conventional structure is originated from B-B tunneling at drain side of channel. The proposed structure, due to the smaller workfunction of metal at drain side, lowers the band bending at channel to drain contact and increases the horizontal distance between conduction and valance bands in this region and reduce the B-B tunneling, considerably. So region 3 of gate metal acts as a filter to prevent

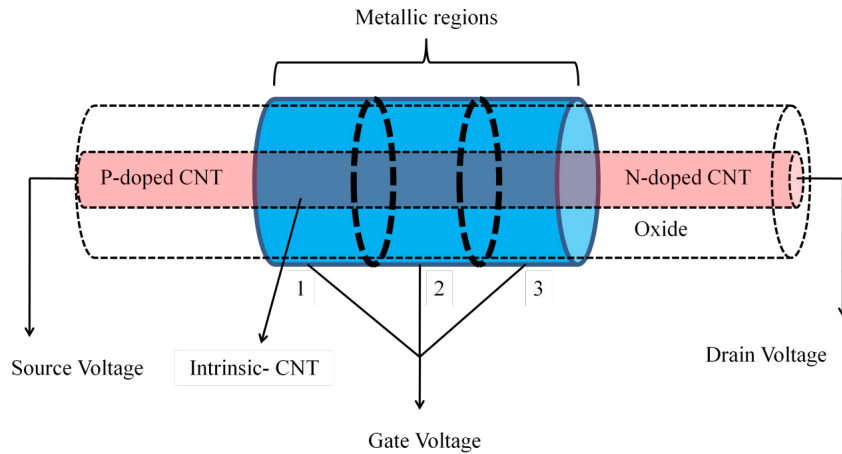


Fig. 1: Schematic view of MSG-T-CNTFET structure.

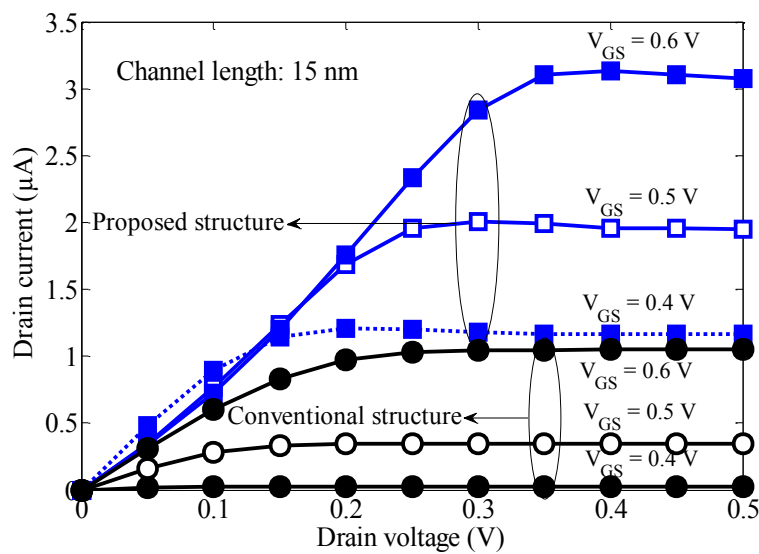


Fig. 2: Output current versus drain source voltage at different gate source voltages.

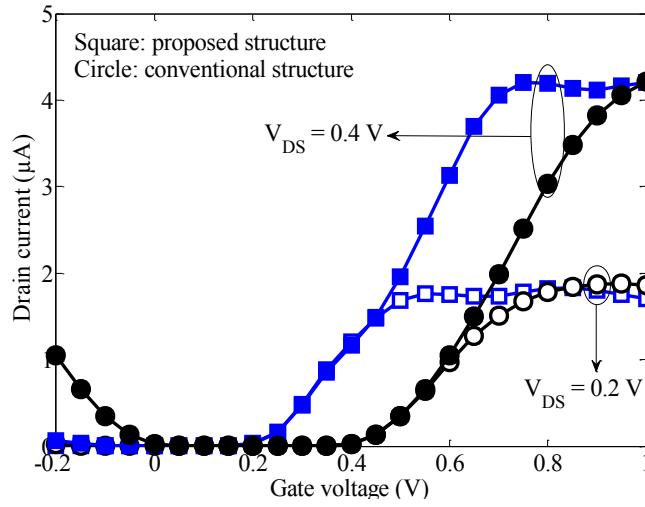


Fig. 3: Output current versus gate source voltage at different drain source voltages.

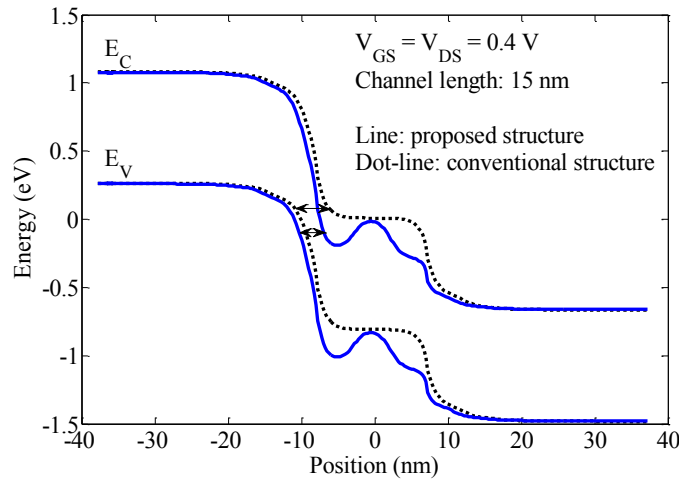


Fig. 4: Energy band diagram along the CNT for MSG and conventional structures at $V_{GS}=V_{DS}=0.4$ V.

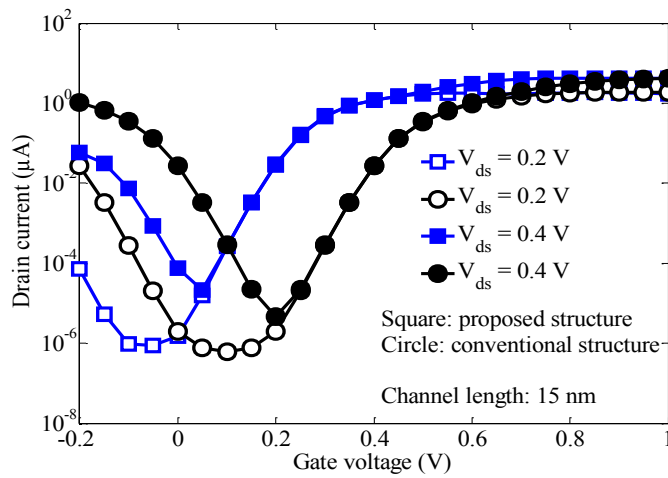


Fig. 5: $I_{DS}-V_{GS}$ characteristics of the structures at different drain source voltages.

the carrier to create the leakage current and improves the OFF regime current and ambipolar behavior.

The magnitudes of electric field for both structures are illustrated in Fig. 7. In conventional FETs, the electric field peak happens at gate to drain or source borders and the breakdown mechanism is started around these borders. The potential is the integral of electric field graph. Increasing the number of peaks lowers their height and so a larger voltage is needed to reach the critical electric field or in another words, the breakdown voltage increases by increasing the number of peaks in the device electric field profile. Also, this technique moderates the hot electron effect. From Fig. 7, it is seen that by applying the MSG

structure additional peaks are created in electric field profile and the maximum peak is reduced. So, our proposed structure can operate at higher voltage biases than conventional structure.

In following simulations we investigate the effects of variations in workfunction and length of regions 1, 2, and 3 on important device characteristics such as saturation current, leakage current, current ratio, transconductance, gate capacitance, and cut-off frequency. These parameters have been evaluated at different channel lengths. At first we study the effects of workfunction difference from 0.1 eV to 0.5 eV. All three sections of gate have the same length. Saturation current variations by channel length have been depicted in Fig. 8(a).

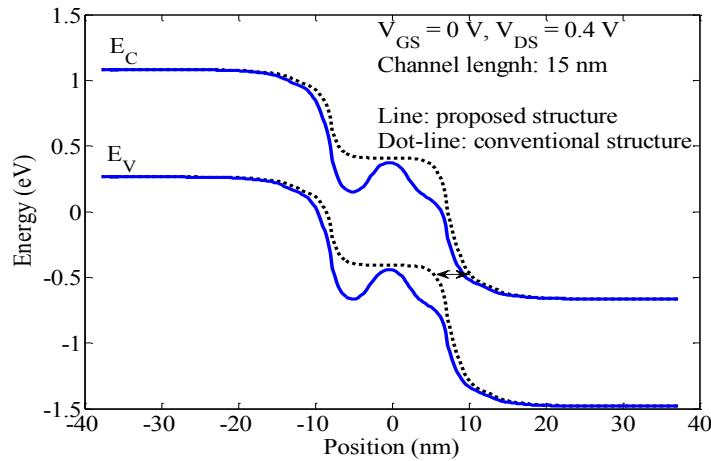


Fig. 6: Energy band diagram along the CNT for MSG and conventional structures at OFF regime.

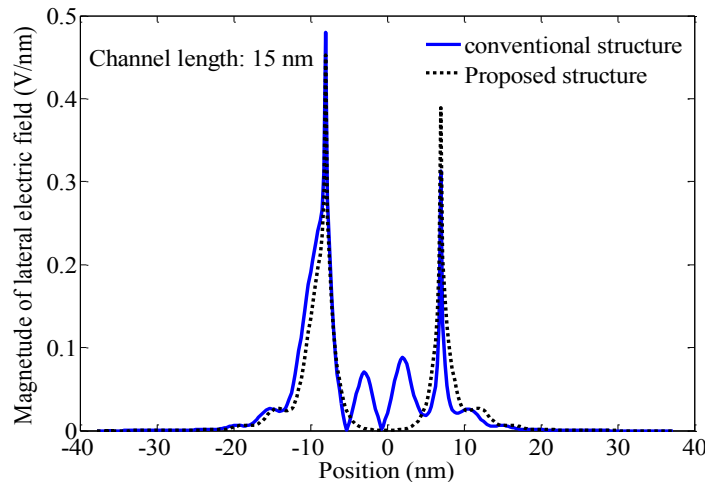


Fig. 7: Electric field distribution along the device for the proposed and conventional structures.

The difference in workfunction of side and middle regions ($\Delta\Phi$) of gate are causes to band bending, and the larger difference the steeper band bending. It is seen that in all workfunction differences the MSG structure provides larger saturation current. Fig. 8(b) illustrates the OFF current variations by channel length. Our proposed structure includes lower leakage currents in all investigated points due to the wider distance between the bands at drain side of channel. The best behavior belongs to the difference of 0.3 eV. ON current and OFF current have been simulated at $V_{GS}=0V, V_{DS}=0.4V$ and $V_{GS}=0.4V, V_{DS}=0.4V$, respectively. ON/OFF current ratio in Fig. 8(c) is extracted from Fig. 8(a, b). The largest ratios are extracted from $\Delta\Phi=0.3\text{ eV}$ because of its minimum leakage current.

One of the challenging issues in the performance of nanoscale devices is their cut-off frequency (F_T). This parameter is calculated by $g_m/(2\pi C_g)$ where g_m is transconductance and C_g is the gate capacitance. Transconductance

shows the potential barrier sensitivity to the gate voltage which is calculated by $\Delta I_D/\Delta V_g|_{V_D}$. Transconductance variations versus gate length are illustrated in Fig. 9(a). MSG-T-CNTFET has better performance than C-T-CNTFET and it is clearer for larger $\Delta\Phi$. Fig. 9(b) shows another effective parameter on cut-off frequency, the gate capacitance. This parameter experiences higher values for larger $\Delta\Phi$. From Fig. 9(a) and 9(b), the transconductance and gate capacitance move in opposite directions to increase and decrease the cut-off frequency, respectively depends on their ratios. Fig. 9(c) illustrates the cut-off frequency at different channel lengths and $\Delta\Phi$ for both structures. MSG structure has better frequencies at channel lengths smaller than 45 nm where increase in transconductance is a dominant factor.

For gate lengths beyond 45 nm, the conventional structure has better performance but their differences are not considerable and cut-off frequencies are close to each other. At

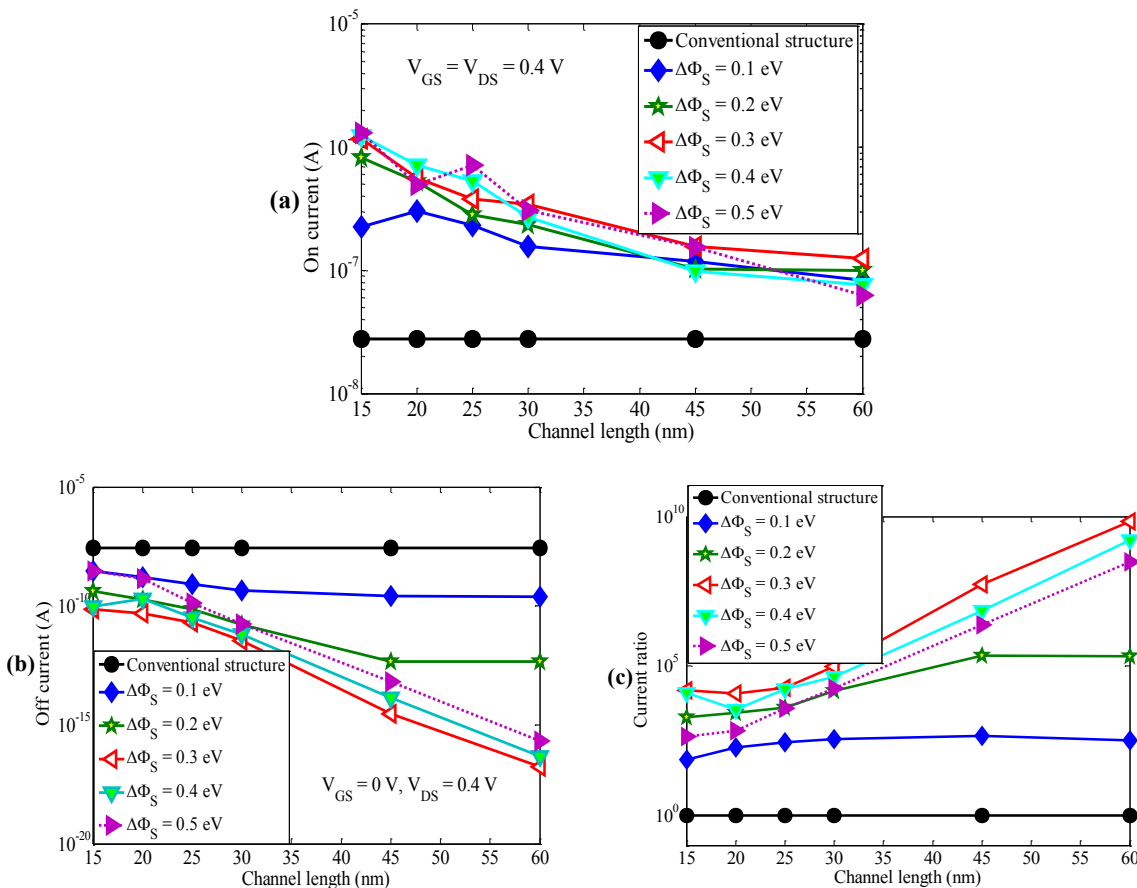


Fig. 8: Variation in (a) Saturation current (b) leakage current and (c) Current ratio, by $\Delta\Phi$ versus channel length for MSG and conventional structures.

shorter channel length, our proposed structure has superior frequency performance such that 15 nm channel length and $\Delta\Phi=0.3$ eV results in 7 times larger cut-off frequency for MSG structure. From figure 8 to 13, it is concluded that the workfunction difference can be selected $\Delta\Phi=0.3$ eV to obtain the more optimized performance.

In next figures, the device parameters are evaluated at different lengths for regions number 1, 2, and 3 while the $\Delta\Phi$ between side regions and central region of gate is fixed at 0.3 eV. Length of

region number 2 which is middle region (L_M), is changed from one third of channel length ($L_C/3$) to $L_C/3+10$ nm. Side metals have equal lengths. Fig. 10(a) shows the variation in saturation current versus main gate length and channel length.

It is seen that where all regions of gate has equal length, i.e. $L_M=L_C/3$, we get the maximum ON current. The OFF state current is investigated in Fig. 10(b). The low value of leakage current for MSG structure in all lengths is observed. Fig. 10(c) shows the current ratio obtained from the

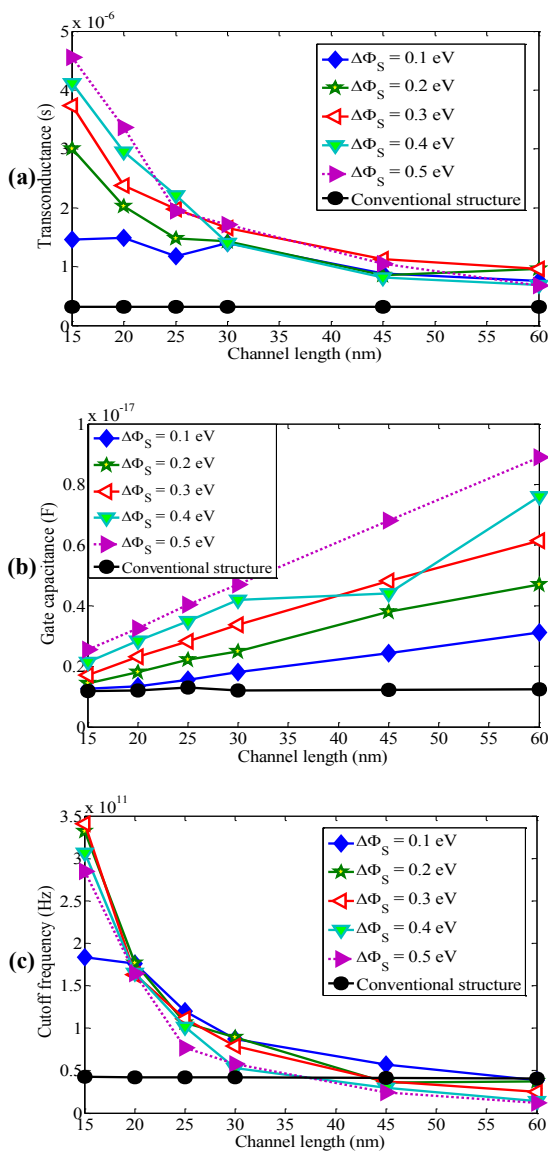


Fig.9: (a) Transconductance (gm) , (b) Gate capacitance, and (c) Cut-off frequency evaluation by $\Delta\Phi$ versus channel length for the proposed and conventional structures.

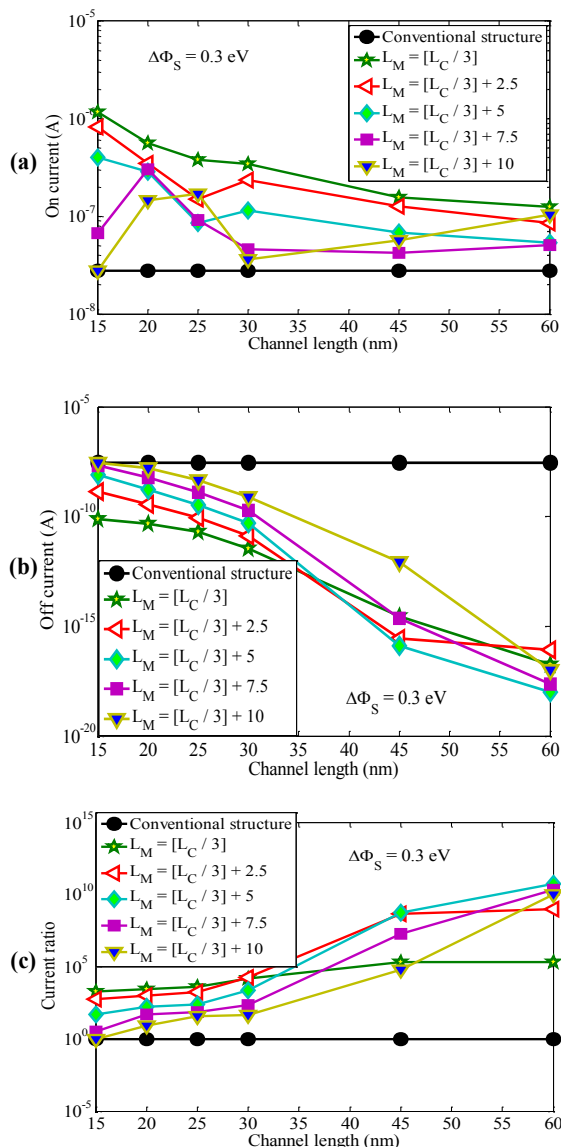


Fig. 10: The effects of side gate length on (a) saturation current, (b) leakage current, and (c) ON/OFF current ratio where the difference in workfunctions is fixed at 0.3 eV.

data presented in Fig. 10 (a and b). Considerable improvement in current ratio is apparent for the proposed structure. Same investigations have been done for cut-off frequency in terms of transconductance and gate capacitance (Fig. 11(a, b and c)). Increase in cut-off frequency shows that our proposed modifications are more efficient for short channel devices such as those results previously seen in improving the other parameters. The cut-off frequency and current ratio variations prove that beside $\Delta\Phi=0.3$ eV, the best length for three metal regions is the equal length.

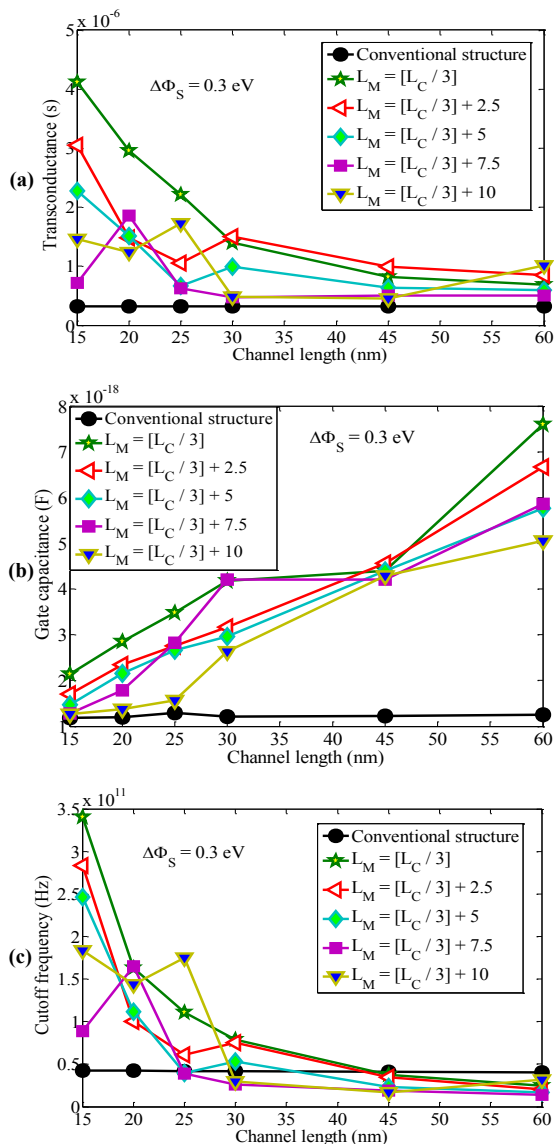


Fig. 11: (a) Transconductance (g_m), (b) Gate capacitance, and (c) Cut-off frequency evaluation by the length of middle gate versus channel length for the proposed and conventional structures.

CONCLUSION

In this paper, by self consistent solution of Poisson and Schrodinger equations within NEGF formalism, MSG-T-CNTFET structure has been proposed and simulated. Our simulations show that the proposed structure by band bending engineering improves the saturation current and ambipolar behavior of the device and increases the current ratio, considerably. Reduction in hot electron effect and increase in cut-off frequency at short channel lengths are other benefits of the MSG structure. Design considerations have been performed on workfunction difference between side metals and the middle gates and their lengths. The 0.3 eV difference between workfunctions and equal length for all three gate sections results in most desired characteristics. From simulations and investigations it can be concluded that the proposed structure is a proper candidate for using the tunneling CNTFETs in digital and high cut-off frequency applications.

CONFLICT OF INTEREST

The authors declare that there is no conflict of interests regarding the publication of this manuscript.

REFERENCES

- [1] Shaker A., Ossaimee M., Zekry A., Abouelatta M., (2015), Influence of gate overlap engineering on ambipolar and high frequency characteristics of tunnel-CNTFET. *Superlat. Microst.* 86: 518-530.
- [2] Tans S., Verschueren A., Dekker C., (1998), Room-temperature transistor based on a single carbon nanotube. *Nature.* 393: 49-51.
- [3] Arefinia Z., Orouji A. A., (2009), Quantum simulation study of a new carbon nanotube field-effect transistor with electrically induced source/drain extension. *IEEE Trans. Device Mater. Reliab.* 9: 237-243.
- [4] Wei W., Lu Z., Xueying W., Zhubing W., Ting Z., Na L., Xiao Y., Gongshu Y., (2014), The combined effects of halo and linear doping effects on the high frequency and switching performance in ballistic CNTFET. *J. Semicond.* 35: 114004-114011.
- [5] Wei W., Na L., Yuzhou R., Hao L., Lifan Z., Jin L., Junjie J., Xiaoping C., Kai W., Chunping X., (2013), A computational study of linear doping on the high-frequency and switching performances of hetero material gate CNTFET. *J. Semicond.* 34: 124002-124007.
- [6] Wei W., Xu M., Liu J., Li N., Zhang T., Jiang S., Zhang L., Wang H., Gao J., (2015), Investigation of hetero-material-gate in CNTFETs for ultra low power circuits. *J. Semicond. Tech. Sci.* 15: 131-144.
- [7] Tahne B. A., Naderi A., (2016), SLD-MOSCNT: Anew MOSCNT with step-linear doping profile in the source and drain regions. *Int. J. Mod. Phys. B.* 30: 1650242-1650242.
- [8] Rahman A., Guo J., Datta S., (2003), Theory of Ballistic Nanotransistors. *IEEE Trans. Electron Devices.* 50: 1853-1864.

- [9] Shokri A. A., Karimi Z., (2014), Electronic band structure of a Carbon nanotube superlattice. *Int. J. Nano Dimens.* 5: 63-67.
- [10] Ziabari S. A. S., Saravani M. J. T., (2017), A novel lightly doped drain and source Carbon nanotube field effect transistor (CNTFET) with negative differential resistance. *Int. J. Nano Dimens.* 8: 107-113.
- [11] Koswatta S. O., Nikonov D. E., Lundstrom M. S., (2005), Computational study of carbon nanotube p-i-n tunnel FETs. *IEDM Tech. Dig.* 518-521.
- [12] Pulfrey D. L., , Chen L., (2009), Comparison of p-i-n and n-i-n carbon nanotube FETs regarding high-frequency performance. *Solid-State Electron.* 53: 935-939.
- [13] Appenzeller J., Lin Y. M., Knoch J., Chen Zh., Avouris Ph., (2005), Comparing carbon nanotube transistors the ideal choice: A novel tunneling device design. *IEEE Trans. Electron Devices.* 52: 2568-2576 .
- [14] Naderi A., Tahne B. A., (2016), T-CNTFET with gate-drain overlap two increased saturation current. *ECS J. Solid State Sci. Technol.* 5: 3032-3036.
- [15] Nagavarapu V., Jhaveri R., Woo J. C. S., (2008), The tunnel source (PNPN) N-MOSFET: A novel high performance transistor. *IEEE Trans. Electron Devices.* 55: 1013-1019.
- [16] Pan A., Chui C. O., (2015), Gate-Induced source tunneling FET (GISTFET). *IEEE Trans. Electron Devices.* 62: 2390-2395.
- [17] Wang H., Chang S., Hu Y., He H., He J., Huang Q., He F., Wang G., (2014), A novel barrier controlled tunnel FET. *IEEE Trans. Electron Devices.* 35: 797-802.
- [18] Kordrostami Z., Sheikh M. H., Zarifkar A., (2012), Influence of channel and underlap engineering on the high-frequency and switching performance of CNTFET. *IEEE Trans. Nanotechnol.* 11: 526-533.
- [19] Naderi A., Keshavarzi P., Orouj A. A. i, (2011), LDC-CNTFET: A carbon nanotube field effect transistor with linear doping profile channel. *Superlat. Microstr.* 50: 145-156.
- [20] Guo J., (2004), Carbon nanotube electronics: Modeling, physics, and applications, Phd thesis, Purdue University.